INFLUENCE OF DIFFERENT RESIDUAL STRESS DISTRIBUTIONS ON FATIGUE CRACK GROWTH

M. Beghini, L. Bertini and E. Vitale *

The results of fatigue crack growth tests conducted on Compact Tension specimens with residual stress fields due to laser welds are presented and discussed. Three distinct residual stress fields were tested in order to induce different crack propagation conditions, including both positive and negative contributions to the Stress Intensity Factor produced by external loading. Experimental data are analysed by means of a non-linear numerical model in order to provide a correct interpretation of observed trends.

INTRODUCTION

The presence of residual stresses can strongly influence the integrity of a machine part, particularly when a significant fatigue damage is expected during operating life. In many cases, residual stresses are an undesired consequence of manufacturing or joining technologies such as welding or cold forming. In other cases they are intentionally produced by means of proper techniques (ex.: shot peening) with the aim of improving fatigue strength.

In recent years a notable research effort has been devoted to the developments of techniques for the quantitative prediction of the residual stress effects on Fatigue Crack Growth (FCG) (see for example Parker (1), Kang et al. (2), Beghini and Bertini (3)). The estimation of fatigue endurance in the presence of residual stress fields for actual components often poses relevant difficulties, as regards both the evaluation of the intensity of such fields and the prediction of their influence on material behaviour. To this end, it has been demonstrated (3) that non-linear effects, due to crack closure phenomena, have to be properly accounted for.

* Dipartimento di Costruzioni Meccaniche e Nucleari, University of Pisa (Italy)

In the present work a previously developed numerical model (3,4) for predicting residual stress effects on fatigue crack growth is applied to the analysis of experimental results obtained with CT specimens in very different residual stress conditions.

RESIDUAL STRESS ANALYSIS

A set of Fatigue Crack Growth (FCG) tests were conducted according to ASTM E647 with Compact Tension (CT) specimens (thickness B=12 mm) machined from an API 5L X65 steel plate (Yield strength: 490 MPa). Some of the specimens, directly cut from the plate, were tested to determine the actual FCG behaviour of the base material. Other specimens were obtained from slabs on which longitudinal laser welds had been performed in order to induce residual stresses. Three distinct weld geometries were employed (see Fig. 1) intended to induce different effects on FCG. A coupled numerical-experimental procedure, developed by the authors (a description can be found in the reference (5)) was applied for the complete determination of residual stress fields, in the three different welding geometries.

For specimens of type S1, compressive residual stresses were detected ahead the notch while the opposite is true for the other two geometries (S2 and S3). The Stress Intensity Factor (SIF) produced by the three residual stress distributions (K_{res}) is shown in Fig. 2 vs. crack length 'a' (measured from the face A in Fig. 1).

For S1 specimens residual stresses tend to close the crack ($K_{res}<0$) and crack edges contact effects have to be expected during fatigue cycles. In these conditions both the effective SIF range (K_{max}-K_{min}) and R^* ratio (K_{min}/K_{max}) differ from the corresponding values due to external loads (nominal values). For the correct determination of the effective conditions at the crack tip, the contact stresses on the crack edges have to be properly considered. This analysis was performed by means of an iterative numerical procedure based on the Weight Function method (3,4). Numerical results are shown in Figs. 3 and 4. It can be observed that the effective SIF range (ΔK_{eff}) is lower than the nominal one for S1 specimens in the whole range of tested crack lengths. The R^* ratio shows a more complex behaviour: for short cracks (a<42 mm) the effective R^* ratio (R^*_{eff}) is less than the nominal one ($R^*=0.1$) while the opposite is true for longer cracks. For S2 and S3 specimens, cracks are always open ($K_{res}>0$) and residual stresses have no effect on the SIF range while a strong modification of the R^* ratio (which is much higher than the nominal value: $R^*=0.1$) is observed.

EXPERIMENTAL RESULTS AND DISCUSSION

Some FCG tests were performed with specimens with no residual stresses (base material). In particular two experimental Fatigue Crack Growth Rate (FCGR) da/dN vs ΔK curves were obtained: the first with $R^*=0.1$ and the second with $R^*=0.5$. Tests were conducted in air applying sinusoidal loading at frequency f=10 Hz under the control of a computer

procedure (Bertini and Vitale (6)) which allowed for the automatic acquisition of applied loadings and crack growth rates during the tests.

Experimental results were fitted using the Erdogan function (Kanninen and Popelar (7)) by which correlation factors higher than 0.98 were obtained for both R^* values; for clarity sake, in the figures, the fitting curves only are reported for the base material. In particular the following values were deduced for the threshold SIF range: ΔK_{th}=6.5 MPa$\sqrt{m}$ for R^*=0.5 and ΔK_{th}=18 MPa$\sqrt{m}$ for R^*=0.1. The Erdogan function was interpolated to predict the FCGR for different values of R^*; in particular, the following relationship (7) was assumed for the ΔK_{th}:

$$\Delta K_{th} = \Delta K_{tho} \cdot (1-R^*)^{\gamma} \qquad (1)$$

where ΔK_{tho} and γ were deduced from the threshold values of the base material.

The FCG tests of welded specimens were conducted under the same nominal conditions (f=10Hz, R^*_{nom}=0.1). In Figs. 5 and 6, the FCGR measured during these tests are plotted vs the nominal ΔK range and compared with the best-fit curves for the base material. It can be observed that specimens S2 and S3 showed FCGRs in the range of the base material curves. In particular short cracks show higher rates (near the R^*=0.5 curve) and for longer cracks the FCGR of S2 specimen is higher than S3. A qualitative explanation of these phenomena can be tried considering the effects of R^* on FCGR. As shown in Fig. 3, the effective R^* ratio was near to 0.5 for short cracks for both S2 and S3 specimens while for longer cracks R^* ratio is higher in S2 specimens.

A more evident discrepancy can be observed between S1 and base material behaviours in Fig. 6. As previously described, in this case residual stresses strongly influence the effective SIF range also. If measured FCGRs are reported vs the effective SIF range the distance from base material curves is reduced as shown in Fig. 7. The difference for smaller cracks can be partially explained considering the effect of the R^* ratio (which vanishes for short cracks in S1 specimens) on the ΔK_{th}. The extrapolated ΔK_{th} value for R^*=0, which can be deduced from eqn. 1 and base materials data, is about 21 MPa$\sqrt{m}$, a value which is in reasonable accordance with the experimental trend. For longer cracks FCGR approaches and overcomes the base material curve (R^*=0.1) and also this fact can be explained considering that for a>42mm R^*_{eff}>0.1 (see Fig. 3).

For S2 and S3 specimens, which showed R^*_{eff} ratios almost always within the base material analysed range, a comparison was made between the observed FCGRs and the rates predicted by the Erdogan law on the basis of the effective ΔK and R^* values. Predicted vs observed values are plotted in Fig. 8 for both specimens.

Similar comparisons for S1 specimens are not yet possible due to the lack of FCGR curves for small R^* ratios. Nevertheless, the fairly

good agreement of the observed ΔK_{th} for S1 specimens with the value extrapolated from Base material data and the accordance shown in Fig. 8 indicate that a reasonable good prediction of residual stress effects on FCG can be obtained if effective values are considered. Further tests are planned in order to obtain a direct measure of ΔK_{th} for small R^* values.

CONCLUSIONS

The effects of different residual stress distributions on FCG were studied by standard CT specimens with laser welds. An accurate analysis of the experimental results was performed on the basis of the knowledge of residual stress fields and applying a non-linear numerical procedure for determining the effective conditions of the crack tip during fatigue cycles. A fairly good description of FCG behaviours was obtained for the specimens with tensile residual stresses employing base material data in the whole range of tested crack length. For specimens with residual compressive effects accurate predictions were obtained both for short and long cracks where extrapolations of base material data can be reasonably performed. These results can be considered a verification of the capability of the numerical model to correctly predict the phenomenon.

REFERENCES

(1) A.P. Parker, Stress Intensity Factors, Crack Profiles, and Fatigue Crack Growth Rates in Residual Stress Fields. Residual Stress Effect in Fatigue, ASTM STP 776, 224-234, ASTM, Philadelphia, (1982).

(2) K.J.Kang,J.H.Song and Y.Y.Earmme, Fatigue crack growth and closure behaviour though a compressive residual stress field, Fatigue Fract. Engng. Mater. Struct., Vol 13, No 1, pp. 1-13, (1990).

(3) M.Beghini and L.Bertini, Fatigue crack propagation through residual stress fields with closure phenomena, to appear on Eng. Fract. Mech.

(4) M. Beghini and L. Bertini, Analytical and Numerical Evaluation of the Residual Stress Effects on Fatigue Crack Propagation, Proc. 4th Int. Conf. on Comp. Methods and Exp. Meas., Comp. Mech. Pub., Southampton (1989).

(5) M.Beghini and L.Bertini , Residual stress modelling by experimental measurements and finite element analysis, to appear on J. for Strain Analysis.

(6) L.Bertini and E.Vitale, A multistation computer-aided material testing system for fracture mechanics and fatigue, Proc. ASME Int. Conf. in Eng.Comp. and Exhib., ASME, New York, Vol. 2, pp. 23-29.

(7) M.F.Kanninen and C.H.Popelar, "Advanced Fracture Mechanics", Oxford Science Series 15,Oxford University Press, New York (1985).

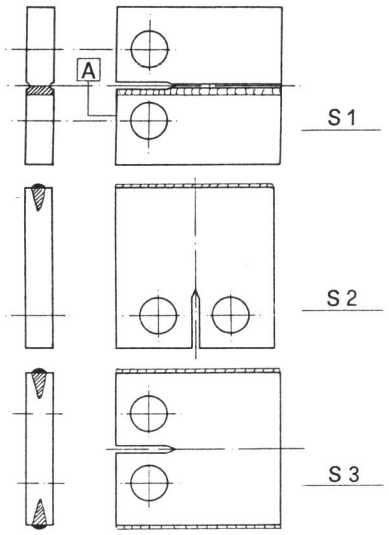

Fig. 1 - Adopted welding geometries for CT specimens.

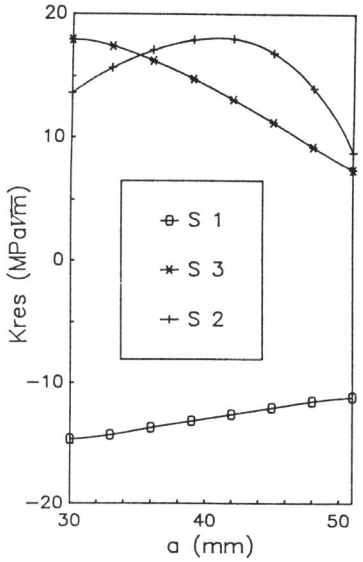

Fig. 2 - Residual SIF curves

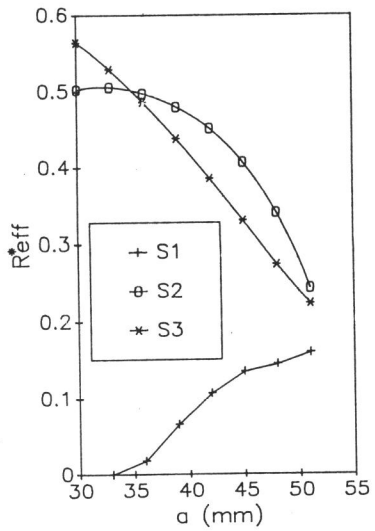

Fig. 3 - Effective R* ratios for the three geometries.

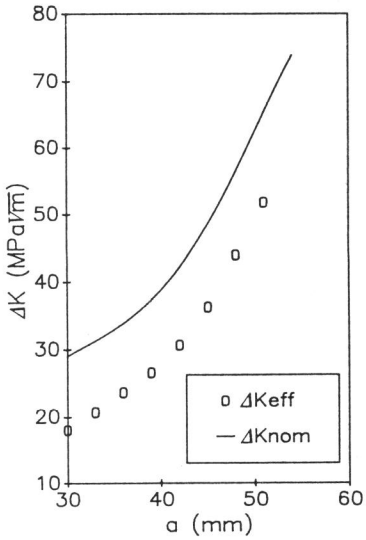

Fig. 4 - Comparison of effective and nominal SIF ranges for S1 specimens.

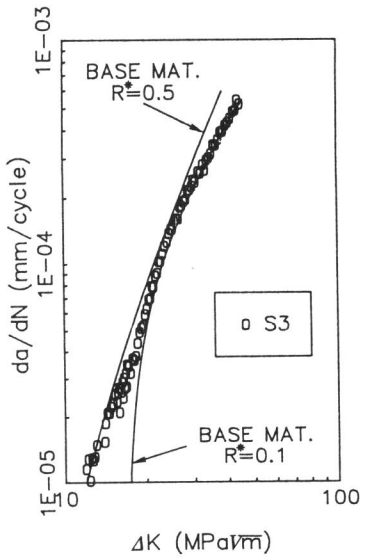

Fig. 5 - FCGR data vs nominal SIF range for S3 and base material.

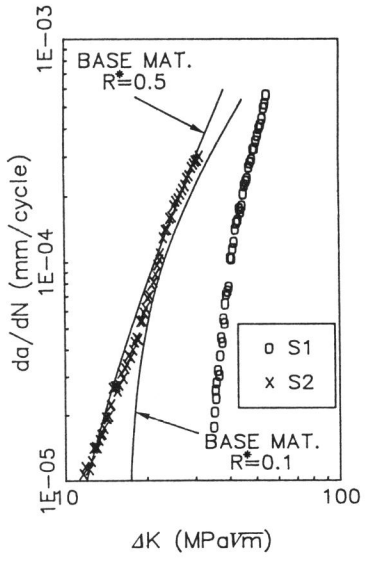

Fig. 6 - FCGR data vs nominal SIF range for S1, S2 and base material.

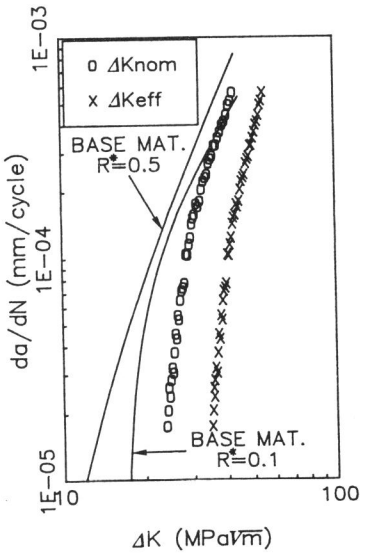

Fig. 7 - FCGR vs nominal and effective SIF range for S1 specimens.

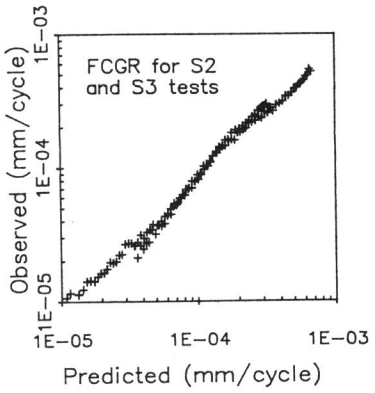

Fig. 8 - Predicted vs measured FCGR for S2 and S3 specimens.